Disturbed State Modeling for Fully Saturated Sand under Dynamic Load

Park, Inn-Joon[*1]
Kim, Soo-Il[*2]

요 지

본 연구에서 제안한 교란상태 개념 (disturbed state concept; DSC)은 변형중인 재료는 상대적으로 손상되지 않은 상태(relative intact state; RI)와 완전히 파괴된 상태(fully adjusted state; FA)가 혼합되어 있다는 기본가정에 기초를 두고 있다. 여기에서 사용된 두 가지 상태, 즉 RI상태와 FA상태는 재료의 파괴정도를 정의하는 기준이 된다. 이와 같은 개념을 바탕으로 DSC는 반복 하중하에 있는 포화사질토의 거동특성에 대한 통합된 구성방정식을 제공한다. 포화사질토에 대한 본 모델의 계수들은 실삼축시험(truly triaxial test)의 결과를 통해 산정된다. 또한 실내실험을 통하여 얻은 결과를 이용하여 본 모델에 대한 검증을 수행하였다. DSC모델을 이용한 역해석과 해석대상 시험결과는 전반적으로 일치되는 경향을 보이고있다.

본 연구의 결과를 토대로, DSC 모델은 동하중하의 포화 사질토의 거동특성을 규명할 수 있다고 사료된다.

ABSTRACT

The disturbed state concept (DSC) proposed here is based on the idea that a deforming material element can be treated as a mixture of two constituent parts in the relative intact (RI) and fully adjusted (FA) states, referred to as reference states. Based on this idea, DSC provides a unified constitutive model for the characteristics of saturated sands under cyclic loading. The model parameters for saturated sands are evaluated by using data from truly triaxial test device. The laboratory test results are also used for the verification of DSC model. In general, the model predictions are found to provide satisfactory correlation with the test results. From the results of this research, it can be stated that the DSC model is capable of

*1 Member, Post-Doctor, Dept. of Civil Engrg., Yonsei Univ.
*2 Member, Professor, Dept. of Civil Engrg., Yonsei Univ.

characterizing the cyclic behavior of saturated sands under dynamic loading.

Keywords : Disturbed state concept, Relative intact state, Fully adjusted state, Truly triaxial test device, Saturated sand, Dynamic loading.

1. Introduction

For modeling the behavior of saturated sands under dynamic load, it is necessary to characterize the dynamic nonlinear behavior of saturated geological materials. Although a number of models have been proposed to characterize behavior of dry geological materials including elastic, plastic, and cyclic loading responses, few constitutive models have been developed for the behavior of fully saturated soils under dynamic loading. Such realistic constitutive models play an important role in analyzing and predicting the response of saturated geological materials.

The purpose of this research is to develop improved model for saturated sands based on a general concept, called the *disturbed state concept* (DSC), that can characterize behavior of saturated soils. The initial idea for this theory was introduced by Desai (1974) to characterize the softening response of an overconsolidated soil by expressing the observed response in terms of its response in its normally consolidated state as the reference state. DSC model has been successfully verified with respect to other materials such as dry sands (Armaleh and Desai, 1990), dry interfaces (Desai and Ma, 1992), saturated clay-steel interface (Rigby and Desai, 1995), saturated sand-steel interface (Alanazy, 1996), and liquefaction of saturated sand and interface (Desai *et al*, 1998; Park, 1997). Furthermore, the model will be calibrated and verified with respect to comprehensive laboratory tests such as truly triaxial test for the saturated Ottawa sands.

2. Disturbed State Concept

In this study, the *disturbed state concept* (DSC) is developed to model the undrained behavior of Ottawa sand subjected to cyclic loading including the effect of liquefaction and stress softening.

In the DSC, it is assumed that applied forces cause disturbance or change in the material' s microstructure. As a result, an initially relative intact (**RI**) material modifies continuously, through a process of natural self-adjustment, and a part of it approaches the *fully adjusted* (**FA**) state at randomly disturbed locations in the material as shown in Fig. 1. Thus, the *observed or average response* can be represented in terms of the responses of the materials in RI and in FA state, which are called reference states as shown in Fig. 2. In this concept, RI state can be characterized as elastic, elastic-perfectly plastic, or any constitutive model like the HiSS model (Desai, 1980; Desai *et al.* 1986, Desai and Wathugala, 1987). FA state can be assumed to imply the state in which the material can continue to carry the shear stress level

reached up to that state under given initial hydrostatic stress and can continue to deform in shear with constant volume-- *critical state* (Roscoe *et al.*, 1957).

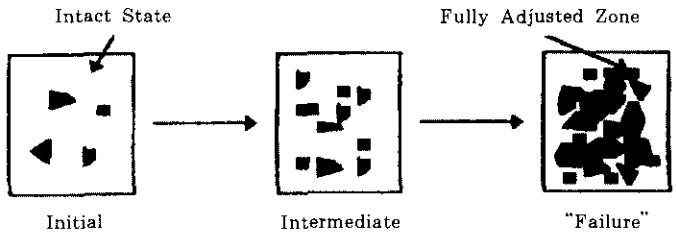

Figure 1 Relative intact and fully adjusted state(Desai, 1992)

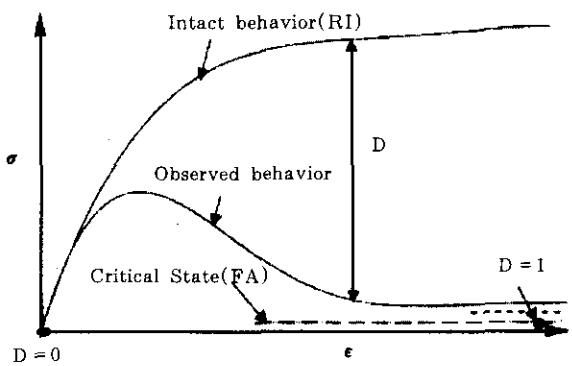

Figure 2 Schematic of stress-strain behavior

2.1 Relative Intact State

Relative intact state in this study is characterized by using an elasto-plastic model that includes only hardening behavior. Here the basic δ_o model in the HiSS Family is used to represent the behavior of the elasto-plastic material in the RI state. The δ_o model is based on *associative plasticity* and *isotropic hardening*. In this model, the single yield surface function (**F**), proposed by Desai *et al* (1986) and Desai and Wathugala (1987) is given by

$$F = \frac{J_{2D}}{P_a^2} - F_b F_s = 0 \qquad (1)$$

where J_{2D} = the second invariant of the deviatoric stress tensor; p_a = atmospheric pressure with

the stress units; F_b = the basic function which describes the shape of $\mathbf{F}$ in the $J_1 - \sqrt{J_{2D}}$ space (see Fig. 3(a)),

$$F_b = -\alpha\left(\frac{J_1 + J_{1s}}{p_a}\right)^n + \gamma\left(\frac{J_1 + J_{1s}}{p_a}\right)^2 \tag{2}$$

F_s = the function which describes the shape of $\mathbf{F}$ in the Octahedral plane (see Fig. 3(b)), and is given by

$$F_s = (1 - \beta S_r)^m \tag{3}$$

S_r = the stress ratio,

$$S_r = \frac{\sqrt{27}}{2}\frac{J_{3D}}{J_{2D}^{3/2}} \tag{4}$$

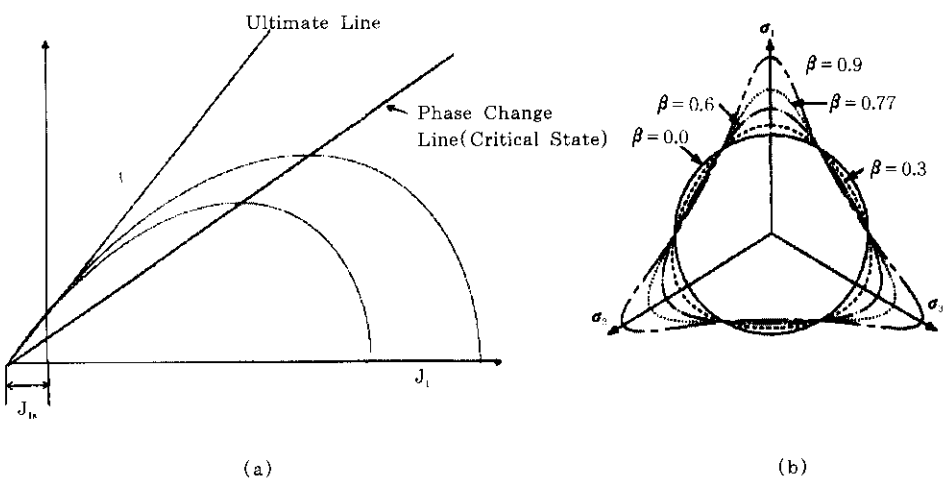

Figure 3 The yield surface of HiSS model

J_1 = first invariant of the stress tensor, J_{3D} = the third invariant of the deviatoric stress tensor, J_{1s} = shift of J_1 axis for materials such as concrete which possess tensile strength (see Fig. 3(a)), n = phase change parameter, γ, β and m = material parameters associated with the ultimate behavior, and m = −0.5 is often used. The hardening function, α, can be defined in terms of the plastic strain trajectory and can be written as:

$$\alpha = \frac{h_1}{\xi_D^{h_2}} \tag{5}$$

where h_1 and h_2 = hardening parameters, ξ_D = the trajectory of deviatoric plastic strains,

$$\xi_D = \int \sqrt{dE_{ij}^p dE_{ij}^p} \tag{6}$$

where dE_{ij}^p = the increment of deviatoric plastic strain tensor,

$$dE_{ij}^p = d\varepsilon_{ij}^p - \frac{1}{3} d\varepsilon_{ij}^p \delta_{ij} \tag{7}$$

From the plasticity theory for the small strains, the total incremental strain can be decomposed into elastic ($d\varepsilon_{ij}^e$) and plastic ($d\varepsilon_{ij}^p$)components as

$$d\varepsilon_{ij} = d\varepsilon_{ij}^e + d\varepsilon_{ij}^p \tag{8}$$

in which the elastic strain increment, $d\varepsilon_{ij}^e$, is related to the stress increment, $d\sigma_{ij}$, by the generalized Hooke's law as

$$d\sigma_{ij} = C_{ijkl}^e d\varepsilon_{kl}^e \tag{9}$$

The plasticity relationship can be derived from equation (8), equation (9), the associative flow rule, $d\varepsilon_{ij}^p = \bar{\lambda} n_{ij}$ and the consistency condition, $dF = 0$, as follows:

$$d\sigma_{ij} = C_{ijkl}^e (d\varepsilon_{kl} - d\varepsilon_{kl}^p) = C_{ijkl}^{ep} d\varepsilon_{kl} \tag{10}$$

where $\bar{\lambda}$ is a scalar factor of proportionality given by

$$\bar{\lambda} = \frac{n_{ij} C_{ijkl}^e d\varepsilon_{kl}}{n_{ij} C_{ijkl}^e n_{kl} - \dfrac{\partial F}{\partial \xi} \left(\dfrac{\partial F}{\partial \sigma_{kl}} \dfrac{\partial F}{\partial \sigma_{kl}} \right)^{1/2}} \tag{11}$$

n_{ij} is a unit normal to yield surface F:

$$n_{ij} = \frac{\dfrac{\partial F}{\partial \sigma_{ij}}}{\left[\dfrac{\partial F}{\partial \sigma_{kl}} \dfrac{\partial F}{\partial \sigma_{kl}} \right]^{1/2}} = \frac{\dfrac{\partial F}{\partial \sigma_{ij}}}{\left\| \dfrac{\partial F}{\partial \sigma_{kl}} \right\|} \tag{12}$$

and C_{ijkl}^{ep} is elasto-plastic constitutive tensor:

$$C_{ijkl}^{ep} = C_{ijkl}^e - \frac{C_{ijrs}^e n_{rs} n_{pq} C_{pqkl}^e}{n_{mn} C_{mnpq}^e n_{pq} - \dfrac{\partial F}{\partial \xi} \left(\dfrac{\partial F}{\partial \sigma_{pq}} \dfrac{\partial F}{\partial \sigma_{pq}} \right)^{1/2}} \tag{13}$$

2.2 Fully Adjusted State

The FA state is modeled by using critical state concept. At the critical state condition, shear deformations can continue indefinitely without further changes in volume. Such critical state often lies on a straight line called critical state line (CSL) with the slope $\bar{m}$ as shown in Fig. 4:

$$\sqrt{J_{2D}^c} = \bar{m} J_1^c \tag{14}$$

During shearing, the materials change in volume and initial void ratio, e_o, changes. Finally, at the critical state the void ratio, e^c, is given by

$$J_1^c = 3p_a \times e^{\left(\frac{e_o^c - e^c}{\lambda}\right)} \tag{15}$$

where e_o^c is the value of critical state of void ratio corresponding to $J_1^c = 3p_a$ and λ is a slope of the critical state line as shown in Fig. 5. In this study, the behavior of the material at the critical state is defined by using equations (14) and (15).

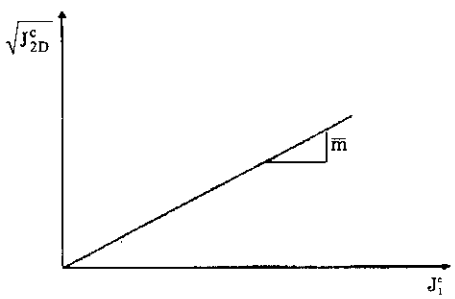

Figure 4 A critical state line on $\sqrt{J_{2D}^c} - J_1^c$ plane

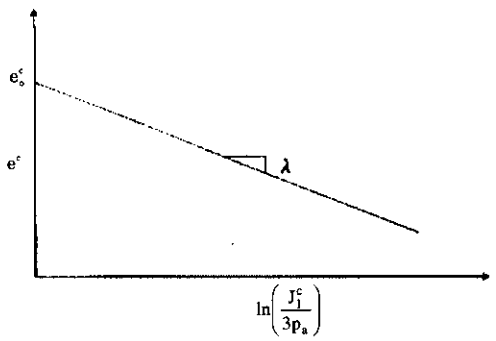

Figure 5 An isotropic compression of sand

2.3 Disturbance Function

The disturbance function can be defined as

$$D = \frac{M_s^c}{M_s} \tag{16}$$

where M_s^c is the mass of solids in the FA state and M_s is the total mass of solids in the materials. Assuming the density of solid particles is constant in time and space, disturbance function, D, becomes

$$D = \frac{V_s^c}{V_s} = \frac{A_s^c}{A_s} \tag{17}$$

where **V** and **A** are volume and area for a constant thickness. Initially with no disturbance the material is assumed to be entirely in the RI state, so D is zero. With full disturbance the material can be assumed to be fully in the FA state, and at the ultimate state, $D = D_u \leq 1$.

Theoretically, the disturbance, D, varies between zero and unity, but many materials fail

before D reaches unity.

The disturbance function, D, used in the current research is given by Armaleh and Desai (1990):

$$D = D_u\left[1 - e^{\left(-A\xi_D^Z\right)}\right] \tag{18}$$

where A, Z, and D_u are material parameters. Fig. 6 shows a schematic of the disturbance function.

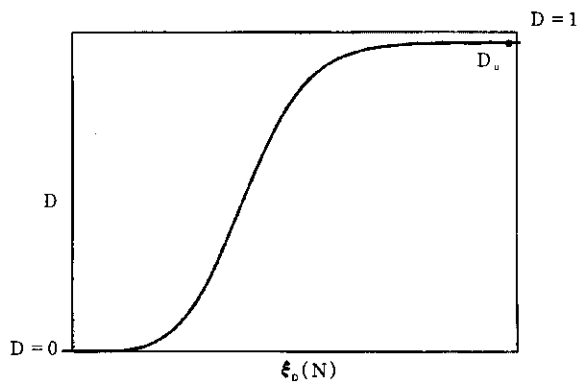

Figure 6 Schematic of DSC function

2.4 Incremental Formulation for the DSC

Based on the equilibrium forces in the observed, RI, and FA states, the incremental constitutive equations to describe the observed response are derived as (Park, 1997; Desai *et al*, 1998)

$$d\sigma_{ij}^a = (1-D)d\sigma_{ij}^i + Dd\sigma_{ij}^c + dD(\sigma_{ij}^c - \sigma_{ij}^i) \tag{19}$$

where superscripts **a**, **i**, and **c** denote observed, relative intact, and critical state, respectively. Substituting Equations (10) and (15) into equation (19), the final incremental relations are derived as

$$d\sigma_{ij}^a = \Omega_{ijkl} \cdot d\varepsilon_{kl}^i + \Psi_{ijkl} d\varepsilon_{kl}^c + dD(\sigma_{ij}^c - \sigma_{ij}^i) \tag{20}$$

If it is assumed that all the strains in each reference state are equal ($d\boldsymbol{\varepsilon}_{ij}^a = d\boldsymbol{\varepsilon}_{ij}^i = d\boldsymbol{\varepsilon}_{ij}^c$), Equation (20) gives the DSC incremental stress-strain equations,

$$d\sigma_{ij}^a = (\Omega_{ijkl} + \Psi_{ijkl})d\varepsilon_{kl}^i + dD(\sigma_{ij}^c - \sigma_{ij}^i) \tag{21}$$

where $\Omega_{ijkl} = (1-D)C^{ep}_{ijkl} + D\frac{\overline{m}}{\sqrt{J^i_{2D}}} J^c_1 \left[\left(C^{ep}_{ijkl} - \frac{1}{3}\delta_{ij} C^{ep}_{mmkl} \right) - \left(\frac{S^i_{ij} S^i_{ij}}{2J^i_{2D}} C^{ep}_{ijkl} \right) \right]$ (22)

$$\Psi_{ijkl} = D\frac{(1+e_o)}{\lambda} J^c_1 \left[\frac{\overline{m} S^i_{ij}}{\sqrt{J^i_{2D}}} + \frac{1}{3}\delta_{ij} \right] \delta_{kl} \tag{23}$$

$$dD = \left[\left(\frac{dD}{d\xi_D} \right) \frac{n_{ij} C^e_{ijkl} \left(n_{ij} n_{ij} - \frac{1}{3} n_{ii} n_{jj} \right)^{1/2}}{n_{ij} C^e_{ijkl} n_{kl} - \frac{\partial F}{\partial \xi} \left(\frac{\partial F}{\partial \sigma_{kl}} \frac{\partial F}{\partial \sigma_{kl}} \right)^{1/2}} \right] d\varepsilon^i_{kl} = R_{ijkl} d\varepsilon^i_{kl} \tag{24}$$

or in the matrix notation,

$$\{d\sigma^a\} = [C^{DSC}]\{d\varepsilon\}^i \tag{25}$$

where

$[C^{DSC}] = [\Omega + \Psi + R^T(\sigma^c - \sigma^i)]$ is the DSC constitutive matrix.

3. Experimental Data on Truly Triaxial Device

The material chosen for the experimental investigation in this research is the Ottawa sand. It is a uniform fine sand with rounded to sub-rounded grains. Some index properties of Ottawa sand are shown in Table 1.

Table 1. General index properties of Ottawa sand

Specific Gravity G_S	Coefficient of Curvature, C_Z	Coefficient of Uniformity, C_U	Maximum Void Ratio, e_{max}	Minimum Void Ratio, e_{min}
2.64	1.6	2.0	0.77	0.46

3.1 Testing Equipment and Test Procedures

For evaluating model parameters, testing equipment used in this study is the truly triaxial device. This apparatus is three-dimensional triaxial stress controlled device with independent control in the three directions. By using this function, it allows three principal stress σ_1, σ_2, and σ_3, and their variations to achieve any stress path in the principal stress space (see Fig. 7). The truly triaxial device consists of the following components: a frame, wall assemblies, deformation measurement system, stress control system, membranes, pore pressure and volume change monitoring system, and data acquisition system. Details about this system are given in the User Manual (Gyi and Desai, 1996).

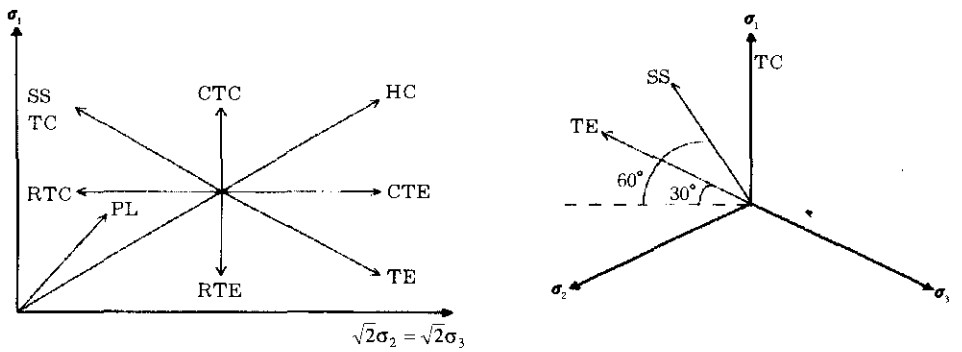

Figure 7 Stress paths followed in truly triaxial device

The cyclic tests are performed when B value is close to 1.0. Additional cell pressure is then applied and the specimen is allowed to consolidate. The specimen is consolidated for at least one hour at the required confining pressure. In this research, the three different confining pressures are used, 69kPa (10psi), 138kPa (20psi), and 207kPa (30psi). Then, the required axial load is applied. Ottawa sand's relative density used throughout this study is 60%. This density is considered as medium dense. The simple test description of cyclic loading type is followed.

Cyclic Loading Test: The cyclic axial load is applied to the specimen with the loading frequency of 0.1 Hz. Cyclic loading is applied by keeping the stresses in x and y direction constant and by changing the stresses in the z direction—axial load. Each cycle composed of a CTC loading path and a RTE loading path (see Fig. 7). These tests are performed under 69kPa, 138kPa, and 207kPa confining pressures. Table 2 shows the total tests performed in this study.

Table 2. Truly triaxial tests on saturated Ottawa sands

Test Number	Type of Loading	Confining Pressure (kPa)	Relative Density(%)	Test Condition
C-1	Cyclic	69	60	Saturated Undrained
C-2	Cyclic	138	60	Saturated Undrained
C-3	Cyclic	207	60	Saturated Undrained
C-4	Cyclic	69	40	Saturated Undrained

3.2 Test Results

Results of cyclic loading tests conducted on fully saturated Ottawa sand samples with the confining pressure of 69, 138, and 207kPa, respectively, are shown in Figs 8 through 10. These test results will be used for evaluating model parameters for the DSC model proposed in

Section 2. Each cycle is made up of a combination of CTC and RTE paths under the frequency of 0.1 Hz. Figs 8(a), 9(a), and 10(a) show the response of excess pore pressure and time. When axial strains reach up to 3 to 6%, excess pore pressure suddenly increases up to initial effective confining pressure (see Figs 8(a), 9(a), and 10(a)). At that time or cycle, initial liquefaction may occur in the saturated samples under cyclic loading. N_{liq} in Figs 8(a), 9(a), and 10(a) refers the number of cycles when initial liquefaction occurs. Figs 8(b), 9(b), and 10(b) represent the response of deviatoric stress, σ_d, and axial stain, ϵ_1. The numbers in these figures refer the number of cycle. For the medium dense sand, these results show that initial liquefaction does not occur until 5th to 8th stress cycles.

It may conclude from test results on medium dense sample of saturated Ottawa sand that the lower the confining pressure, the earlier liquefaction occurs.

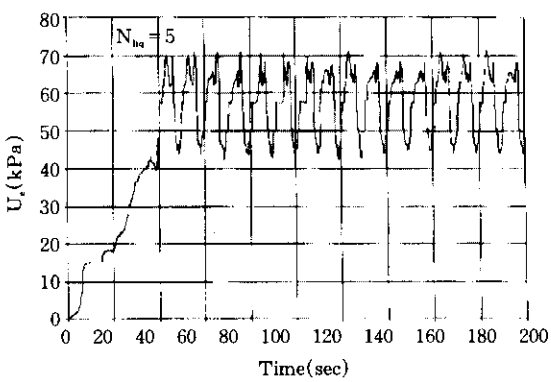

Figure 8(a) Plot of excess pore pressure vs. time for $\bar{\sigma}_0$=69kPa and D_r=60%

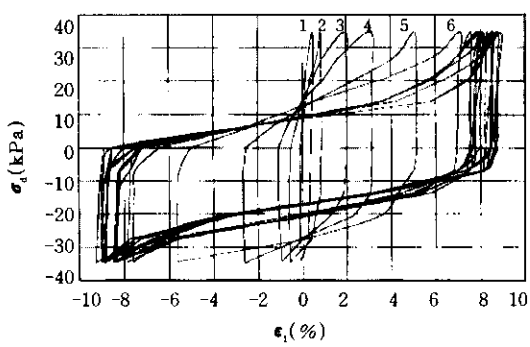

Figure 8(b) Plot of deviatoric stress and axial strain for $\bar{\sigma}_0$=69kPa and D_r=60%

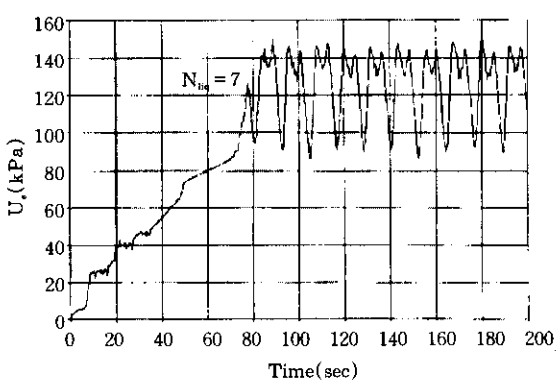

Figure 9(a) Plot of excess pore pressure vs. time for $\bar{\sigma}_0$=138kPa and D_r=60%

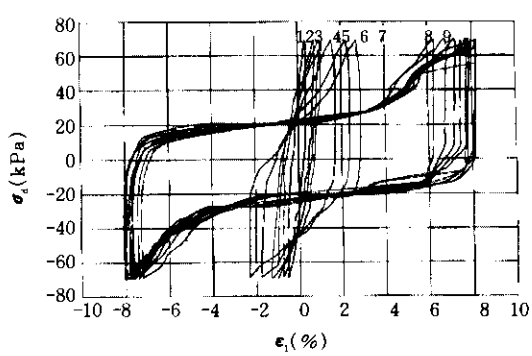

Figure 9(b) Plot of deviatoric stress vs. time for $\bar{\sigma}_0$=138kPa and D_r=60%

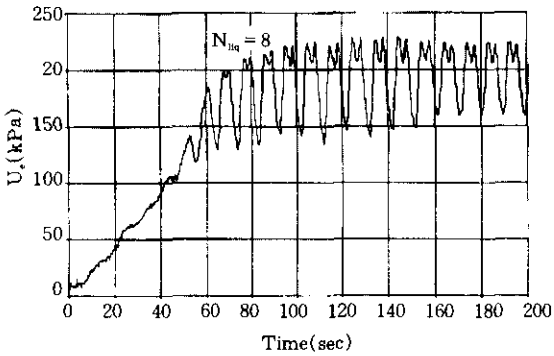

Figure 10(a) Plot of excess pore pressure vs. time for $\bar{\sigma}_0$ = 207kPa and D_r = 60%

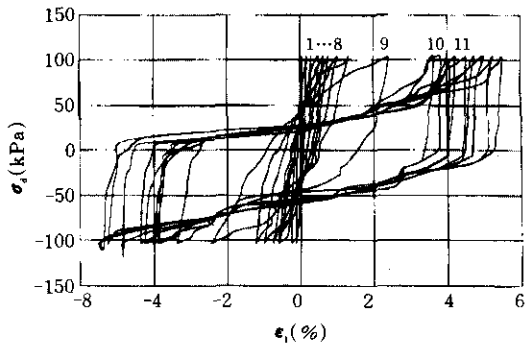

Figure 10(b) Plot of deviatoric stress and axial strain for $\bar{\sigma}_0$ = 138kPa and D_r = 60%

4. DSC Model Parameters and Validation

4.1 DSC Model Parameters

The proposed DSC model involves a number of material constants and they can be determined from a series of cyclic triaxial tests referred in Section 3 (see C-1 to C-3 in Table 2). The material constants can be divided into four categories: the elastic parameters, the parameters for the RI state, the parameters for the FA state, and the parameters for describing

Table 3. Summary of DSC parameters

Material State	Group of Parameters	Parameters	Ottawa Sand
Relative Intact State	Elastic Parameters	E	193000(kPa)
		ν	0.380
	Plastic Parameters	γ	0.123
		β	0.000
		m	-0.500
		n	2.450
		h_1	0.8450
		h_2	0.0215
Fully Adjusted State	Critical State Parameters	$\bar{m}$	0.1500
		λ	0.02
		e_0^c	0.601
Observed State	Disturbance Function Parameters	D_u	0.99
		Z	0.43
		A	4.22

disturbance function. The material parameters are all listed in the following:

1. Elastic Parameters: E and ν 2. RI state parameters: γ, β, n, h_1, and h_2; 3. FA state parameters: $\bar{m}$, λ, and e_o^c; 4. Disturbance Function parameters: D_u, Z, and A.

There are thirteen parameters needed for the proposed model. The procedure of finding parameters for saturated cohesionless soil under dynamic load is developed by author and co-workers (Park, 1997; Desai *et al*, 1998). The DSC model constants obtained from truly triaxial test data for saturated Ottawa sands are given in Table 3.

4.2 Verification of DSC Model

In this section, verification of DSC model with respect to laboratory test data for Ottawa sand is presented. Back predictions are made and the following graphs are plotted to compare observed data with prediction: observed and predicted excess pore pressure, u_e, versus time, *t*. The model predictions are obtained by *POROUS_D* program developed by Desai and co-workers (Desai, *et al*, 1993; Desai *et al*, 1997). The DSC model is implemented in program *POROUS_D* by using equation (25).

4.2.1 Verification of Excess Pore Pressure-Time Response for Ottawa Sand

Figs 11 to 13 show comparison of predicted and observed excess pore pressure, u_e, for three different initial confining pressures, $\bar{\sigma}_o$, as mentioned before.

From the results, the excess pore pressure responses for cyclic loading tests are back predicted very well. Specifically, the predicted and observed time (cycle) when initial liquefaction occurs according to the traditional criterion--u_e equals initial effective confining stress.

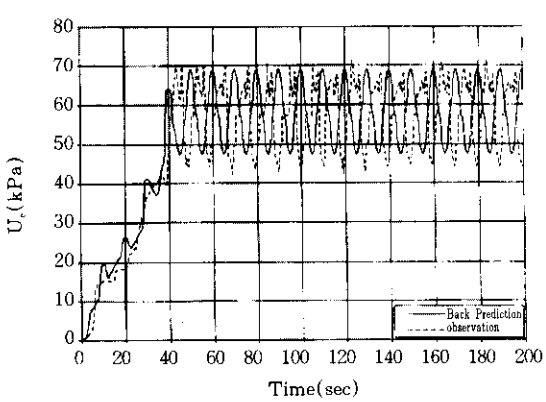

Figure 11 Back predicted excess pore pressure vs. time response of cyclic loading test for $\bar{\sigma}_o$=69kPa

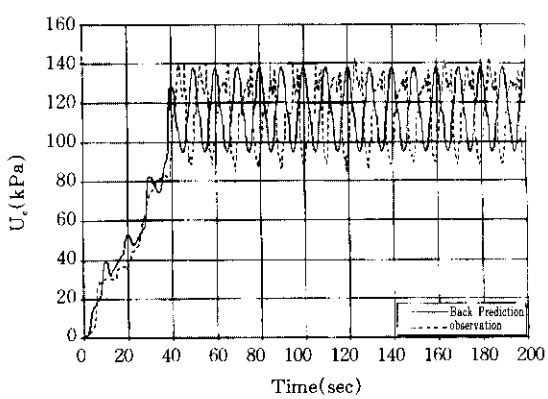

Figure 12 Back predicted excess pore pressure vs. time response of cyclic loading test for $\bar{\sigma}_o$=138kPa

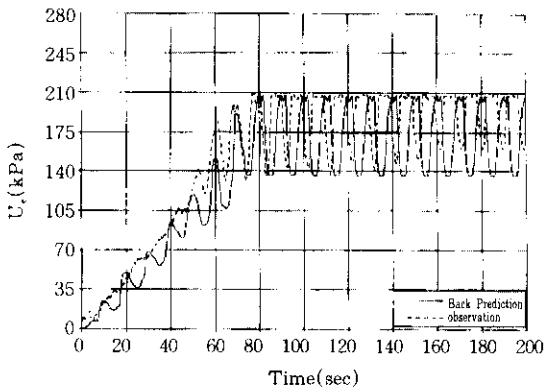

Figure 13 Back predicted excess pore pressure vs. time response of cyclic loading test for $\bar{\sigma}_0 = 207$kPa

4.2.2 Back Prediction of Independent Test

Figs 14 to 16 show predictions of a cyclic test under a constant initial effective confining pressure of 69kPa and a relative density of 40% (see C-4 in Table 2). This test is not used for the determination of parameters. The average parameters given in Table 3 are used for back prediction of this test.

Fig. 14 shows the comparison between observation and prediction for effective mean stress responses. Fig. 15 shows the comparison between observation and prediction for excess pore pressure responses. Finally, Fig. 16 presents the comparison between observation and prediction for Disturbance versus ξ_D.

Overall, the correlation is good. However, there are differences between observations and predictions. These differences can be due to the fact that the parameters were found from tests with different density.

The predicted trends for effective stress, excess pore pressure, and disturbance over the entire test compare well with the observed data.

5. Summary and Conclusions

In the study herein, the DSC model has been introduced as a general concept that involves modeling of saturated cohesionless materials by using two reference states of the material: RI state where the material is assumed to be associative isotropic hardening and FA state where the material is assumed to experience no volume change under further shearing.

Comprehensive laboratory tests have been performed on samples with a relative density, 60%, and three different confining pressures; 69kPa, 138kPa, and 207kPa, respectively. These are done successfully by conducting truly triaxial tests that cover saturated medium dense sand, Ottawa

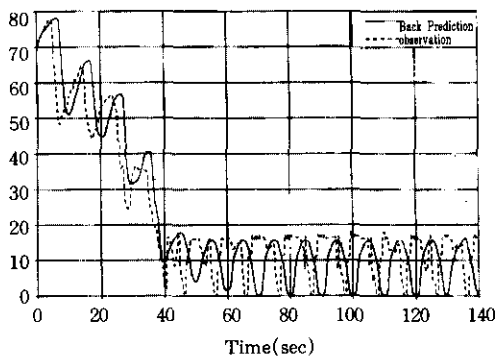

Figure 14 Back predicted effective mean stress vs. time for independent test $\bar{\sigma}_0$=69kPa and D_r=40%

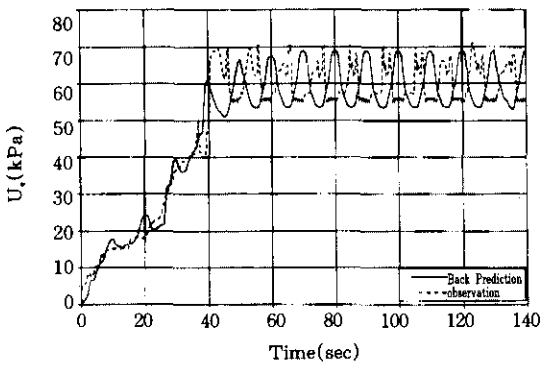

Figure 15. Back predicted of excess pore pressure vs. time for independent test $\bar{\sigma}_0$=69kPa and D_r=40%

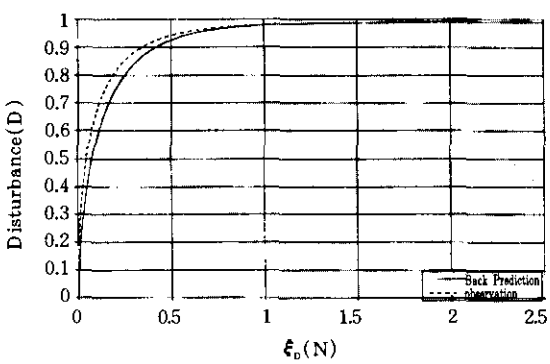

Figure 16 Back prediction of disturbance(D) vs. ξ_D for independent test $\bar{\sigma}_0$=69kPa and D_r=40%

sand, and by introducing the influence of initial confining pressure through the DSC model parameters.

Verification of DSC model in this study is done with respect to fully saturated Ottawa sand. It is shown that the DSC model provides satisfactory results for prediction of the observed behavior. Therefore, DSC model is defined as a powerful and realistic constitutive model for modeling saturated sands under dynamic load.

Reference

1. Alanazy, A. S. (1996) "Testing and Modeling of Sand-Steel Interfaces Under Static and Cyclic

Loading," *Ph.D. Dissertation*, Dept. of Civil Engrg. And Engrg. Mech., Univ. of Arizona, Tucson, Arizona.

2. Armaleh, S. H. and Desai, C. S. (1990) "Modeling Include Testing of Cohesionless Soils Under Disturbed State Concept," *Report to the NSF*, Dept. of Civil Engrg. And Engrg. Mech., Univ. of Arizona, Tucson, Arizona.
3. Desai, C. S. (1974) "A Consistent Finite Element Technique for Work-Sofening Behavior," *Proc. Int. Conference on Computational Methods in Nonlinear Mechanics*, Univ. of Texas at Austin, Austin, Texas.
4. Desai, C. S. (1980) "A General Basis for Yield, Failure, and Potential Functions in Plasticity," *Int. J. Num. Analyt. Meth. In Geomech.*, Vol. 4, pp. 361-375.
5. Desai, C. S. and Ma, Y.(1992) "Modeling of Joints and Interfaces Using the Disturbed State Concept," *Int. J. Num. Analyt. Meth. In Geomech.*, Vol. 16, No. 9, pp. 623-653.
6. Desai, C. S., Park, I. J., and Shao, C.(1998) "Fundamental Yet Simplified Model for Liquefaction Instability," *Int. J. Num. Analyt. Meth. In Geomech.*, in press.
7. Desai, C. S., Somasundaram, S., and Frantziskonis, G. (1986) "A Hierarchical Approach for Constitutive Modeling of Geologic Materials," *Int. J. Num. Analyt. Meth. In Geomech.*, Vol. 10, No. 3, pp. 225-257.
8. Desai, C. S., Shao, C., and Park, I. J. (1997) "Disturbed State Modeling of Cyclic Behavior of Soils and Interfaces in Dynamic Soil-Structure Interaction," *Proc., 9t^h IACMAG Conference*, Wuhan, China.
9. Desai, C. S., and Wathugala, G. W. (1987) "Hierarchical and Unified Modles for Solids and Discontinuities (Joints/Interfaces)," *Short Course Notes*, Workshop on Implementation of Constitutive Laws of Engineering Materials, Dept. of Civil Engrg. And Engrg. Mech. Univ. of Arizona, Tucson, Arizona, pp. 9-10, 31-124.
10. Gyi, M. M. and Desai, C. S. (1996) "User Manual of the Servo-Controlled Cubical Device with Automatic Data Acquisition System," *Report*, Dept. of Civil Engrg. And Engrg. Mech., Univ. of Arizona, Tucson, Arizona.
11. Park, I. J. (1997) "Disturbed State Modeling for Dynamic and Liquefaction Analysis," " Ph.D. Dissertation, Dept. of Civil Engrg. and Engrg. Mech., Univ. of Arizona, Tucson, Arizona.
12. Rigby, D. B. and Desai, C. S. (1995) "Testing, Modeling, and Application of Saturated Interfaces in Dynamic Soil-Structure Interaction," *Report to the NSF*, Dept. of Civil Engrg. And Engrg. Mech., Univ. of Arizona, Tucson, Arizona.
13. Roscoe, K. H., Schofield, A. and, Wroth, C. P. (1957) "On the Yielding of Soils," *Geotechnique*, Vol. 8, pp. 22-53.

(received on Apr. 13. 1998)